Plagioclase archives of depleted melts in the oceanic crust Supplementary Material

David A. Neave[1,2] and Olivier Namur[3]

[1]*Department of Earth and Environmental Sciences, The University of Manchester, M13 9PL Manchester, UK*

[2]*Leibniz Universität Hannover, Institut für Mineralogie, 30167 Hannover, Germany*

[3]*Department of Earth and Environmental Sciences, KU Leuven, BE-3001 Leuven, Belgium*

PHASE EQUILIBRIA EXPERIMENTS

Starting materials

The Háleyjabunga and Stapafell lavas are amongst the most geochemically extreme primitive basalts from Iceland in terms of their major element, trace element and isotopic compositions, which makes them excellent model systems for exploring the consequences of mantle-derived chemical variability on magmatic evolution (Gurenko and Chaussidon, 1995; Maclennan, 2008). The lavas are thought originate from lithologically distinct mantle sources, with the incompatible-element-depleted Háleyjabunga lava being generated following high-degree melting of an initially fertile but latterly refractory peridotite and the Stapafell lava being largely generated by modest-degree melting of a recycled, fusible and modally enriched (i.e., clinopyroxene-rich) peridotite (Shorttle and Maclennan, 2011; Neave et al., 2018). Of key relevance here is that the Háleyjabunga lava is relatively Ca- and Al-rich (i.e., high Ca#, where Ca# = molar Ca/(Ca+Na)) while the Stapafell lava is relatively Fe- and Na-rich (i.e., low Ca), which results in fundamentally different phase equilibria between the two compositions (Neave et al., 2019b).

The synthesis of starting materials is described in detail by Neave et al. (2019b) and summarized below. Natural glass compositions from Condomines et al. (1983), Gurenko and Chaussidon (1995) and Peate et al. (2009) were corrected to the same initial melt MgO content of ~10.5 wt.%. Starting materials with these corrected compositions were then synthesized from reagent-grade oxide and carbonate powders that were fused twice in Pt crucibles at 1600 °C at the Institut für Mineralogie of the Leibniz Universität Hannover, Germany. Platinum crucibles were quenched in H_2O after each fusion to ensure the production of homogenous glasses.

Experimental methods

Crystallization experiments were performed in an internally heated pressure vessel (IHPV) at the Institut für Mineralogie of the Leibniz Universität Hannover, Germany, using methods described in detail by Husen et al. (2016) and Neave et al. (2019b) and summarized below. Approximately 50 mg of each powdered starting material was loaded into $Au_{80}Pd_{20}$ capsules that had first been treated to contain 0.25–0.30 wt.% Fe to minimize Fe exchange with capsule materials (e.g., Gaetani and Grove, 1998). Capsules were suspended from a Pt wire in

the hot zone of the IHPV. Experiments were performed at either 100 MPa or 600 MPa in an Ar pressure medium, and at temperatures that ranged from 1140 to 1240 °C. Experimental conditions are summarized in Supplementary Table 1. Pressure was monitored with a strain gauge manometer and did not vary by more than 5 MPa during the course of the experiments. Temperature was monitored with four unsheathed S-type thermocouples spaced across the hot zone and was typically within 5 °C of the target temperature. Experimental temperatures were approached by heating the furnace from room temperature to 10 °C below the target temperature at a rate of 50 °C/min; final heating was performed at a rate of 10 °C/min to avoid overshooting. Experimental durations varied from 48 hours for near- and super-liquidus experiments to 120 hours for lower-temperature experiments. Experimental products were quenched by fusing the Pt wires on which capsules were suspended, thereby dropping them into a cold zone at the base of the vessel.

Analytical methods

The major element content of experimental products was determined by electron probe microanalysis (EPMA) with a Cameca SX100 instrument at the Institut für Mineralogie of the Leibniz Universität Hannover, Germany. Silicon, Ti, Al, Cr, Fe, Mn, Mg, Ca, Na, K and P were measured in glasses with a beam size of 10 µm, an accelerating voltage of 15 kV and a current of 10 nA. Silicon, Ti, Al, Cr, Fe, Mn, Mg, Ca, Na and K were measured in minerals with a beam size of 1 µm, an accelerating voltage of 15 kV and a current of 15 nA. Gold, Pd and Fe were measured in capsules with a beam size of 1 µm, an accelerating voltage of 15 kV and a current of 40 nA. Elements were counted on peak for 20 s, with the exceptions of Si and Na that were counted on peak for 10 s to minimize drift and Na migration. Background counting times were half on-peak counting times. The following standards were used for calibration: wollastonite (Si and Ca), TiO_2 (Ti), Al_2O_3 (Al), Cr_2O_3 (Cr), Fe_2O_3 (for Fe in silicates and Cr-spinel), Fe metal (for Fe in capsules), Mn_3O_4 (Mn), MgO (Mg), albite (Na), orthoclase (K), apatite (P), Au metal (Au) and Pd metal (Pd).

To ensure internal consistency across multiple sessions, analyses were normalized as follows: glass analyses were normalized to VG-2 basalt glass (NMNH 111240-52; using the preferred MgO content); clinopyroxene, low-Ca pyroxene and plagioclase analyses were normalized to Kakanui augite (NMNH 122142; using preferred values); olivine analyses were normalized to San Carlos olivine (NMNH 111312-44); and chromite analyses were normalized to Tiebaghi Mine chromite (NMNH 117075) (Jarosewich et al., 1980). Accuracy and precision were monitored by measuring the following standards that were also normalized for each analytical session: A-99 basaltic glass (NMNH 113498), Ney County Cr-augite (NMNH 164905) and Lake County plagioclase (NMNH 115900) (Jarosewich et al., 1980, 1987). Major (>1 wt.%) and minor (<1 wt.%) elements were determined with accuracies better than 2% and 10%, and 1σ precisions better than 2% and 15% respectively. Analyses of standards are provided alongside analyses of experimental products in the Supplementary Data. Compositions of experimentally produced glasses and plagioclase crystals are summarized in Supplementary Fig. 1.

Glass H_2O contents were determined in experimental products with low crystal contents by Fourier-transform infrared (FTIR) spectroscopy with a Bruker IFS88 instrument at the Institut für Mineralogie of the Leibniz Universität Hannover, Germany, following the methods described by Husen et al. (2016). In short, H_2O contents were determined in ~100-µm thick wafers using the peak attributed to the OH stretch vibration (3550 cm^{-1}) using a molar absorption coefficient of 68 L/mol cm. Measured glass H_2O contents varied from 0.45 to 0.91 wt.%; all analyses are provided in the Supplementary Data.

Experimental oxygen fugacities

All experiments were conducted under nominally dry conditions (no H_2O was added to dried starting materials), which resulted in melt H_2O contents of 0.56–0.91 wt.% following the reduction of Fe_2O_3 in the starting glasses to FeO and the inward diffusion of trace H_2 from the Ar pressure medium at high temperatures. Colorimetric analyses of experimental products with low crystal contents performed with the approach of Schuessler et al. (2008) returned $Fe^{3+}/\Sigma Fe$ values of 0.13–0.23, which correspond to oxygen fugacity(fO_2) conditions expressed with respect to the fayalite-magnetite-quartz (FMQ) buffer of FMQ+0.2 to FMQ+1.3 (Kress and Carmichael, 1991). Capsule compositions record broadly similar conditions of FMQ+0.0 to FMQ+1.2 (Barr and Grove, 2010). Estimated fO_2 conditions are provided in the Supplementary Data and summarized on Supplementary Table 1.
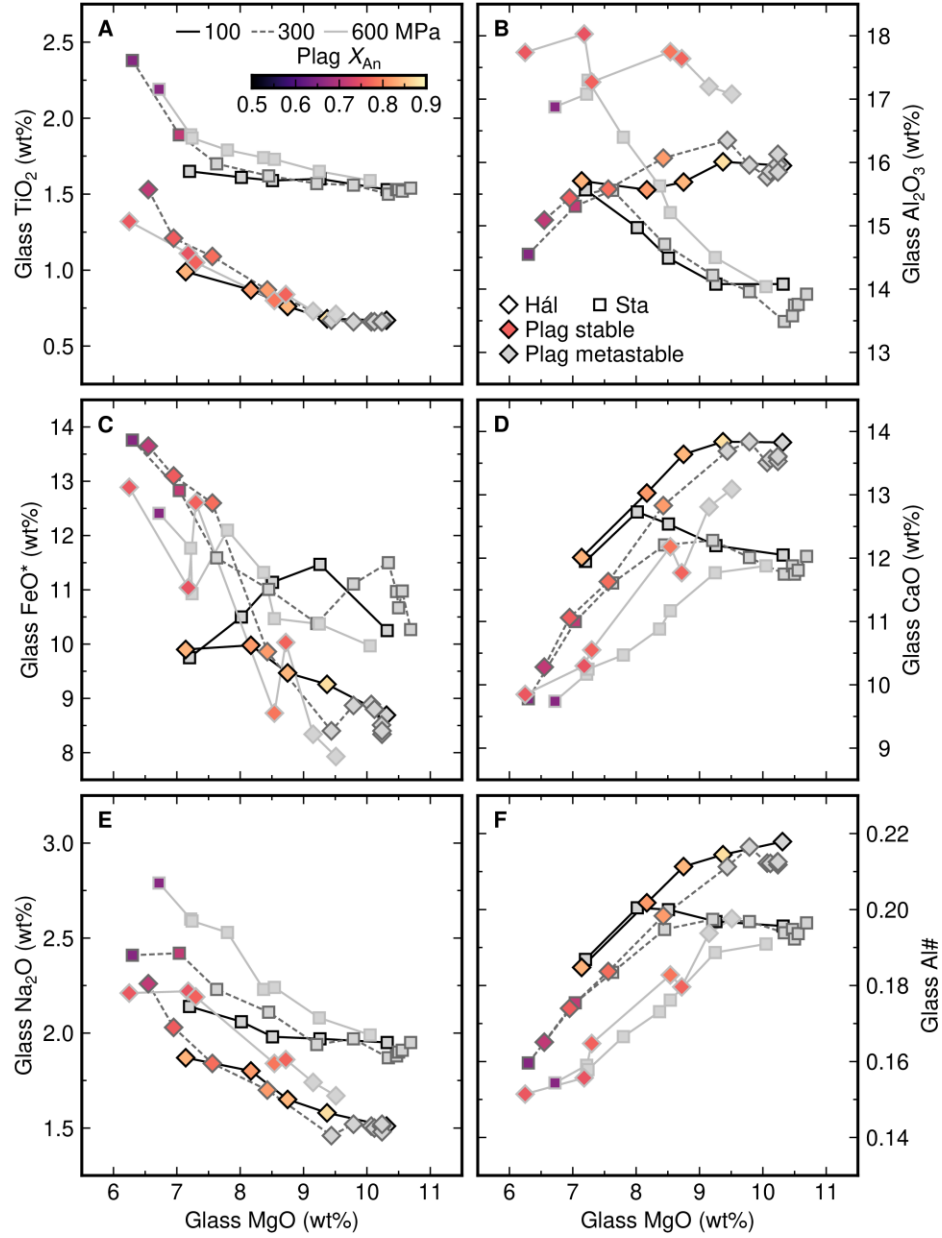
Supplementary Figure 1 Plagioclase-liquid equilibria in synthetic analogues of the high-Ca# Háleyjabunga (Hál) and low-Ca# Stapafell (Sta) lavas from Iceland summarized in terms of glass MgO content versus (A–E) a range of glass major element contents and (F) glass Al# (where Al# = molar Al/(Al+Si)); Fig. 1 in the main text shows equivalent plots for glass Ca# (where Ca# = molar Ca/(Ca+Na)) and glass molar Ca/Al. New results at 100 and 600 MPa are presented alongside results at 300 MPa from Neave et al. (2019b).

Experiment-Capsule ID	Starting composition[1]	P (MPa)	T (°C)	t (hours)	ΔFMQ KC91[2]	ΔFMQ BG10[3]	Fe loss (%)[4]	H_2O[5]	Assemblage[6]
Y0192-6	HAL-X-01A	100	1220	48	0.72	0.45	0.4	0.64	gl
Y0187-2	HAL-X-01A	100	1200	48	0.86	0.88	2.2	0.45	gl - ol - plag
Y0186-11	HAL-X-01A	100	1180	72		1.11	0.3		gl - ol - plag - cpx
Y0185-12	HAL-X-01A	100	1160	120		0.91	-0.7		gl - ol - plag - cpx
B0188-4	HAL-X-01A	100	1140	120		0.66	-3.8		gl - ol - plag - cpx
B0149-11	HAL-X-01A	600	1240	48	0.25	0.00	-7.9	0.72	gl - cpx
B0151-3	HAL-X-01A	600	1220	48		0.50	-5.8		gl - cpx
B0155-5	HAL-X-01A	600	1200	48		0.49	-7.0		gl - plag - cpx
B0184-8	HAL-X-01A	600	1200	48		0.67	0.3		gl - plag - cpx
B0198-10	HAL-X-01A	600	1180	72		0.76	2.7		gl - plag - cpx - low-Ca px
B0183-3	HAL-X-01A	600	1160	96		0.56	-6.8		gl - plag - cpx - low-Ca px
B0187-7	HAL-X-01A	600	1140	96		1.13	1.1		gl - plag - cpx - low-Ca px
Y0192-7	STA-X-01B	100	1220	48	1.32	0.85	-5.2	0.77	gl
Y0187-3	STA-X-01B	100	1200	48	1.34	1.19	5.8	0.55	gl - Cr-sp - ol
Y0186-4	STA-X-01B	100	1180	72		1.17	3.6		gl - ol
Y0185-10	STA-X-01B	100	1160	120		0.79	-1.7		gl - ol - cpx
B0188-5	STA-X-01B	100	1140	120		0.70	-8.4		gl - ol - cpx
B0149-4	STA-X-01B	600	1240	48	0.81	0.55	-10.0	0.91	gl - cpx
B0151-4	STA-X-01B	600	1220	48		0.60	-8.2		gl - cpx
B0155-11	STA-X-01B	600	1200	48		0.60	-9.5		gl - cpx
B0184-7	STA-X-01B	600	1200	48		0.91	-3.2		gl - cpx
B0167-4	STA-X-01B	600	1180	72		0.88	-0.4		gl - cpx - low-Ca px
B0198-12	STA-X-01B	600	1180	72		0.53	4.8		gl - cpx - low-Ca px
B0183-5	STA-X-01B	600	1160	96		0.40	-6.5		gl - cpx - low-Ca px
B0187-6	STA-X-01B	600	1140	96		0.91	4.0		gl - plag - cpx - low-Ca px

Supplementary Table 1 Summary of experimental conditions and products. [1]HAL-X01A, Háleyjabunga lava (high-Ca#); STA-X-01B, Stapafell lava (low-Ca#). [2]Oxygen fugacity calculated from liquid $Fe^{3+}/\Sigma Fe$ using the model of Kress and Carmichael (1991) with respect to the fayalite-magnetite-quartz (FMQ) buffer. [3]Oxygen fugacity calculated from capsule compositions using the model of Barr and Grove (2010) with respect to the fayalite-magnetite-quartz (FMQ) buffer. [4]Relative Fe loss (or gain) to (or from) $Au_{80}Pd_{20}$ capsules determined by mass balance. [5]H_2O contents determined by FTIR. [6]Phase assemblage of experimental products: gl, glass; ol, olivine; cpx, plag, plagioclase; cpx, clinopyroxene; and low-Ca px, low-Ca pyroxene.

PREDICTING PLAGIOCLASE-LIQUID EQUILIBRIA
Rationale and data sources

Empirical models for predicting plagioclase-liquid equilibria and equilibrium plagioclase anorthite contents (X_{An}, where X_{An} = molar Ca/(Ca+Na+K)) are typically calibrated across large ranges of melt composition (Namur et al., 2012 and references therein). While such global calibrations facilitate internally consistent modelling across diverse situations they can also result in lower accuracy and precision than can be achieved by calibrating and applying models under more restricted conditions. Moreover, for technical reasons, the majority of published phase equilibria experiments have been performed at 0.1 MPa (i.e., 1 atm), meaning that plagioclase-liquid equilibria models are generally better constrained at pressures lower than those at which the majority of crustal magmatism takes place (Namur et al., 2012). Here we present a new empirical model optimized for predicting plagioclase-liquid equilibria in oceanic basalts evolving under crustal pressure and temperature conditions.

Calibration data (n = 98) were sourced from relatively recent studies on H_2O-poor (typically <1 wt.%) oceanic tholeiites at a range of pressures (0.1–700 MPa) that report high quality EPMA data. Specifically, data were sourced from experiments on ocean island basalts (OIBs) from Iceland (Neave et al., 2019a, 2019b; this study), mid-ocean-ridge basalts (MORBs) and plagioclase-saturated MORB liquids (Kohut and Nielsen, 2003; Voigt et al., 2017), and oceanic plateau basalts from Shatsky Rise (Husen et al., 2016). Only data from experimental runs containing <50 wt.% glass were used in the calibration to ensure that plagioclase and liquid pairs had approached equilibrium as closely as reasonably possible. The distribution of plagioclase X_{An} in the calibration dataset is summarized in Supplementary Fig. 2A which is analogous to Fig. 2 in the main text.

Test data (n = 36) to independently verify regression quality were sourced from studies on H_2O-poor oceanic and continental tholeiites at range of pressures (0.1–1000 MPa). Specifically, data were sourced from experiments on MORBs (Grove et al., 1992; Yang et al., 1996) and continental tholeiites from Snake River Plain (Whitaker et al., 2007, 2008). The distribution of plagioclase X_{An} in the test dataset is summarized in Supplementary Fig. 2B which is analogous to Fig. 2B in the main text.
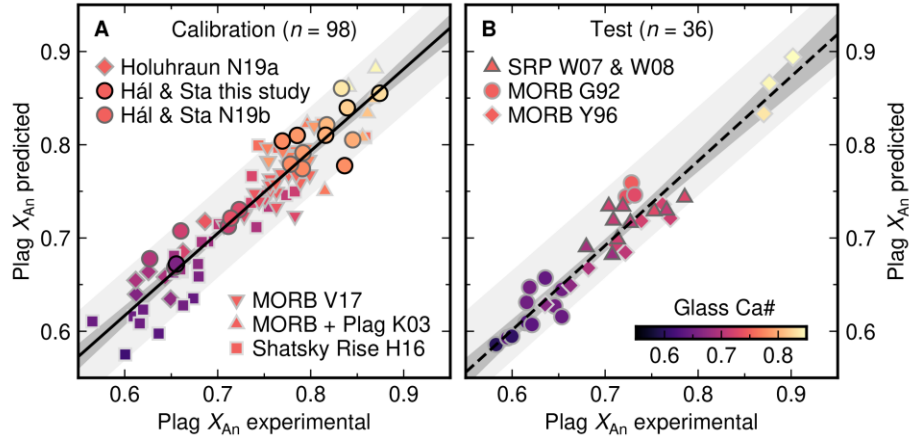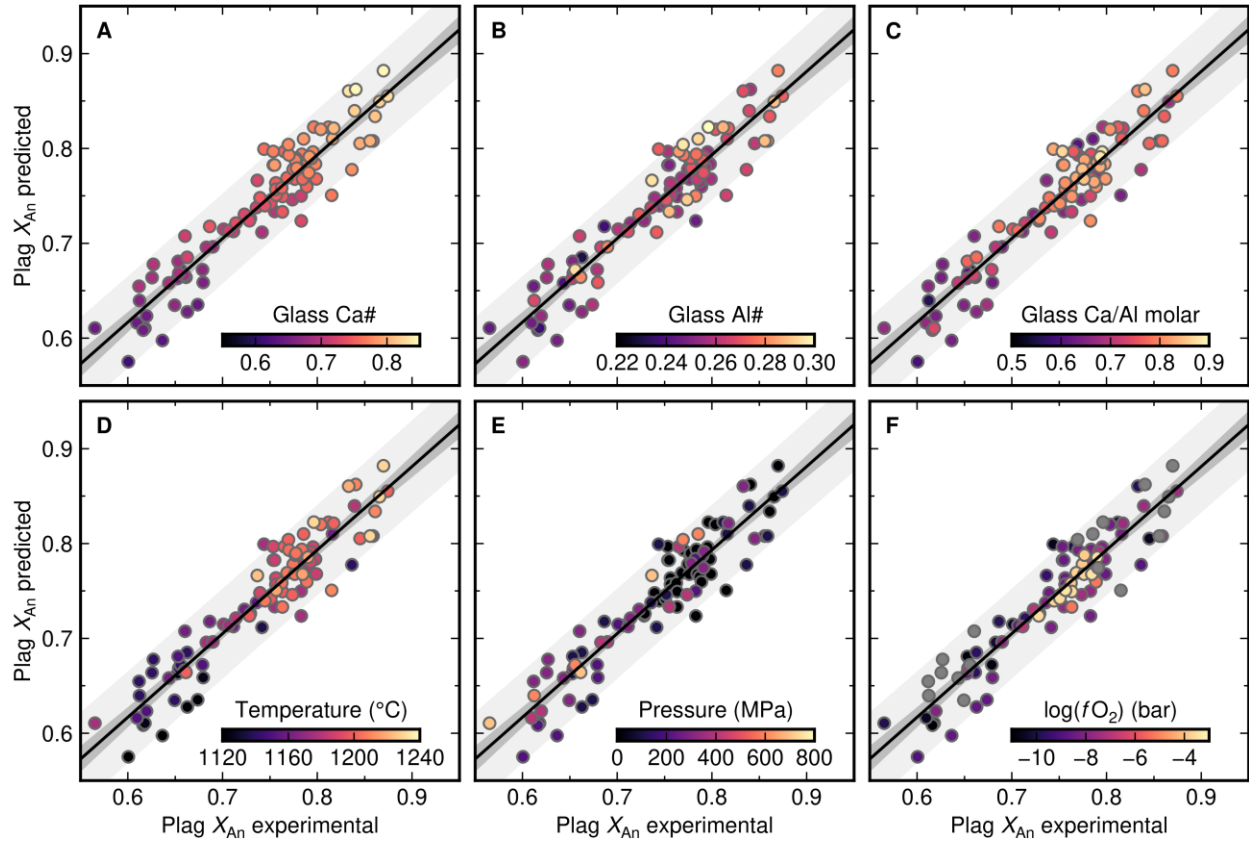
Supplementary Figure 2 (A) Performance of the multiple linear regression (Eq 1) used to predict plagioclase (plag) anorthite content (X_{An}, where X_{An} = molar Ca/(Ca+Na+K)) as a function melt composition. The black line shows a regression through calibration data from experimental studies on basalts from an ocean island, mid-ocean ridges and an oceanic plateau. Dark and pale grey envelopes show 95% confidence and prediction intervals, respectively. Data sources: N19a, ocean island basalts (OIBs) from Holuhraun in Iceland (Neave et al., 2019a); this study, OIBs from Háleyjabunga (Hál) and Stapafell (Sta) in Iceland at 100 and 600 MPa N19b, OIBs from Háleyjabunga (Hál) and Stapafell (Sta) in Iceland at 300 MPa (Neave et al., 2019b); V17, mid-ocean-ridge basalt (MORB) (Voigt et al., 2017); plagioclase-saturated MORB (Kohut and Nielsen, 2003); and oceanic plateau basalts from Shatsky Rise (Husen et al., 2016). (B) Performance of Eq 1 on test data from mid-ocean ridges and a continental hotspot. The dashed black line and dark grey envelope show a regression through the test data and its 95% confidence interval, respectively; the pale grey envelope shows the 95% prediction interval of Eq 1. Data sources: MORB (Grove et al., 1992; Yang et al., 1996); and continental tholeiites from Snake River Plain (SRP) (Whitaker et al., 2007, 2008).

Regression strategy

Least-squares multiple linear regression was then performed using the lm() function in R (R Development Core Team, 2016). The regression equation was selected by trial and error (e.g., Putirka, 2008). Namely, melt compositional parameters were variably combined and both overall r^2 values and p-values of individual regression parameters were evaluated until the following equation was identified (1σ values of regression coefficients are given in parentheses):

$$X_{An} = 0.92(0.07) \cdot Ca\#_{melt} + 1.63(0.24) \cdot Al\#_{melt} + 0.24(0.05) \cdot (molar\ Ca/Al)_{melt} - 0.54(0.06),\ (1)$$

where Ca# = molar Ca/(Ca+Na) and Al# = molar Al/(Al+Si). All regression coefficients are highly significant ($p < 0.001$), and the regression is robust ($r^2 = 0.88$; standard error = 0.025). Adding further compositional parameters such as melt MgO or K_2O contents did not improve the quality of the fit. The standard error of our new model (0.025) is considerably better than the standard errors of the literature models reviewed by Namur et al. (2012), which range from 0.044 to 0.090, though our model is only calibrated for oceanic basalts that are relatively poor in H_2O; the new models of Namur et al. (2012) have comparable standard errors of ~0.030. Relationships between experimental X_{An}, predicted X_{An}, melt composition and other intrinsic conditions (pressure, temperature and oxygen fugacity) are summarized in Supplementary Fig. 3.

Supplementary Figure 3 Performance of the multiple linear regression (Eq 1) used to predict plagioclase (plag) anorthite content (X_{An}, where X_{An} = molar Ca/(Ca+Na+K)) as a function melt composition. The black line shows a regression through calibration data from experimental studies on basalts from an ocean island, mid-ocean ridges and an oceanic plateau and. Dark and pale grey envelopes show 95% confidence and prediction intervals, respectively. Data are colored as follows: (A) glass (i.e., melt) Ca#, where Ca# = molar Ca/(Ca+Na); (B) glass Al#, where Al# = molar Al/(Al+Si); (C) glass molar Ca/Al; (D) temperature; (E) pressure; and (F) oxygen fugacity (fO₂). Experiments for which fO₂ values were not reported are shown in grey.

While the strong dependence of predicted X_{An} on Ca#$_{melt}$ is clear in Supplementary Fig. 3A, it is also important to note that experiments are well reproduced across a wide range of intrinsic conditions relevant to the evolution of oceanic basalts (Supplementary Figs 3D–3F). The possible underestimation of X_{An} in the coolest experiments is of little significance for our study that focusses on the significance of high-X_{An} plagioclase crystals.

A simple linear regression through the test data reveals a similarly strong relationship between experimental and predicted X_{An} as observed for the calibration data ($r^2 = 0.92$; standard error = 0.020). Moreover, relationships between experimental X_{An}, predicted X_{An}, melt composition and other intrinsic conditions in the test dataset are comparable to those in the calibration dataset (Supplementary Fig. 4). Importantly, Eq 1 reliably captures the high-X_{An} compositions reported from some experiments.
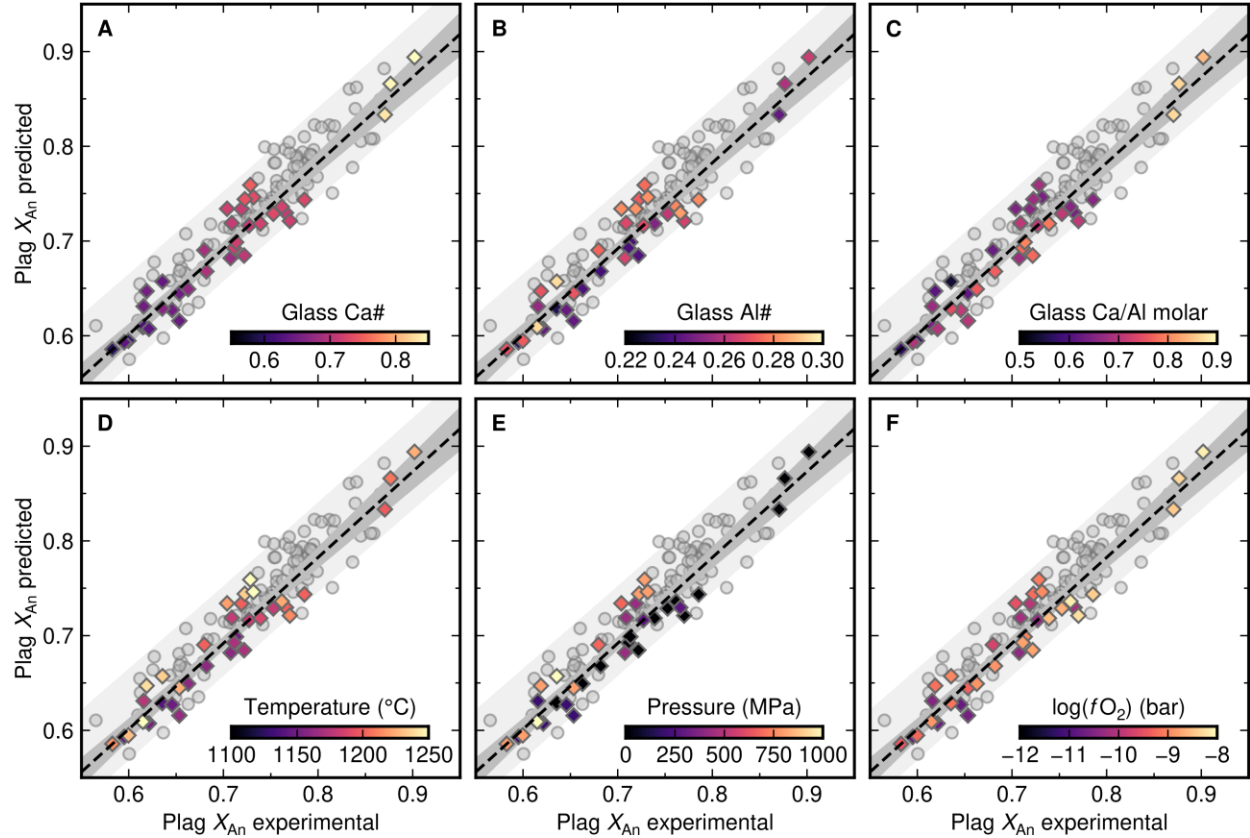
Supplementary Figure 4 Performance of Eq 1 on test data from mid-ocean ridges and a continental hotspot. The dashed black line and dark grey envelope show a regression through the test data and its 95% confidence interval, respectively; the pale grey envelope shows the 95% prediction interval of Eq 1. Regression and test data are respectively shown as grey circles and diamonds colored as follows: (A) glass (i.e., melt) Ca#, where Ca# = molar Ca/(Ca+Na); (B) glass Al#, where Al# = molar Al/(Al+Si); (C) glass molar Ca/Al; (D) temperature; (E) pressure; and (F) oxygen fugacity (fO$_2$).

Verifying plagioclase stability

Although Eq 1 can reliably predict the plagioclase X_{An} in equilibrium with oceanic basalts, it does not account for plagioclase stability. That is, it will return metastable equilibrium plagioclase X_{An} values for melt compositions that are plagioclase undersaturated. Predicted values of plagioclase X_{An} were filtered for plagioclase stability using the following criterion from Gale et al. (2014):

$$K_{d\ An} \times An_{liq} + K_{d\ Ab} + Ab_{liq} = 1. \ (2)$$

Values of An_{liq} and Ab_{liq} were determined from glass compositions while $K_{d\ An}$ and $K_{d\ Ab}$ were predicted from regressions analogous in form to Eq 1 (r^2 = 0.82 and 0.42, respectively). Natural glasses were then determined to be saturated in plagioclase if the value of Eq 2 was within the 95% confidence interval of values estimated from plagioclase-saturated experiments. That is, plagioclase was considered stable when Eq 2 returned 1.00±0.03, which allows some tolerance

for both analytical and fitting uncertainties. As for predicting plagioclase-liquid equilibria we favoured this empirical approach over using thermodynamic models such as the MELTS algorithm (Ghiorso and Sack, 1995) to avoid making potentially erroneous assumptions about crystallization conditions.

PLAGIOGLASE IN OCEANIC BASALTS AND THE OCEANIC CRUST
Data sources

High-X_{An} plagioclase crystals occur throughout the oceanic realm. They are often major constituents of basalts from ocean islands and slow- to intermediate-spreading mid-ocean ridges (Lange et al., 2013), as well as cumulates from ophiolites and the lower oceanic crust (Browning, 1982; Lissenberg et al., 2013). Here we collated data from diverse studies on oceanic samples that report high-X_{An}. We explicitly did not incorporate data from arc settings where elevated X_{An} contents likely result from elevated melt H_2O contents initially suppressing plagioclase crystallization (Sisson and Grove, 1993).

Mineral data are rarely reported in consistent ways between different studies. For example, some studies only report macrocryst (i.e., phenocryst) compositions while others also consider microcryst and groundmass compositions; some separate core and rim analyses while others provide no textural information. In order to maximize our collated data of natural oceanic plagioclase compositions we therefore collated all available data, texturally constrained or not. Sources of natural plagioclase compositions are summarized in Supplementary Table 2.

Setting	Location	Sources	*n*
OIB	Iceland, Eastern Volcanic Zone	Passmore (2009), Neave et al. (2013), Neave et al. (2014) and Caracciolo et al. (2020)	2166
OIB	Iceland, Northern Volcanic Zone	Maclennan et al. (2003)	373
OIB	Galápagos	Cullen et al. (1989) and Stock et al. (2020)	974
OIB	Réunion	Valer et al. (2017)	14
OIB	Kerguelen	Annell et al. (2007)	20
MORB	Mid-Atlantic Ridge	Lange et al. (2013)	299
MORB	Southwest Indian Ridge	Lange et al. (2013)	383
MORB	Juan de Fuca Ridge	Lange et al. (2013)	68
MORB	Gakkel Ridge	Lange et al. (2013) and Bennett et al. (2019)	3969
Ophiolite	Samail Ophiolite, Oman	Browning (1982) and Koga et al. (2001)	98
Lower oceanic crust	East Pacific Rise, especially Hess and Pito Deeps	Constantin et al. (1996), Lissenberg et al. (2013) and Faak and Gillis (2016)	318
Lower oceanic crust	16.5°N Oceanic Core complex on the Mid-Atlantic Ridge	Sanfilippo et al. (2019) (porphyroblasts inherited from primary igneous textures only)	4

Supplementary Table 2 Sources of natural plagioclase data summarized in Fig. 4

REFERENCES CITED IN SUPPLEMENTARY MATERIAL

Annell, H., Scoates, J.S., Weis, D., and Giret, A., 2007, Petrology of flood basalts at the tholeiitic-alkalic transition and phenocryst compositions, Mt. Marion Dufresne, Kerguelen Archipelago, Southern Indian Ocean: Canadian Mineralogist, v. 45, p. 809–835, doi:10.2113/gscanmin.45.4.809.

Barr, J.A., and Grove, T.L., 2010, AuPdFe ternary solution model and applications to understanding the $f\mathrm{O}_2$ of hydrous, high-pressure experiments: Contributions to Mineralogy and Petrology, v. 160, p. 631–643, doi:10.1007/s00410-010-0497-z.

Bennett, E.N., Lissenberg, C.J., and Cashman, K. V., 2019, The significance of plagioclase textures in mid-ocean ridge basalt (Gakkel Ridge, Arctic Ocean): Contributions to Mineralogy and Petrology, v. 174, p. 49, doi:10.1007/s00410-019-1587-1.

Browning, P., 1982, The petrology, geochemistry and structure of the plutonic rocks of the Oman ophiolite: Open University, 404 p., doi:10.21954/ou.ro.0000de14.

Caracciolo, A., Bali, E., Guðfinnsson, G.H., Kahl, M., Halldórsson, A., Hartley, M.E., and Gunnarsson, H., 2020, Temporal evolution of magma and crystal mush storage conditions in the Bárðarbunga-Veiðivötn volcanic system, Iceland: Lithos, p. 105234, doi:10.1016/j.lithos.2019.105234.

Condomines, M., Grönvold, K., Hooker, P.J., Muehlenbachs, K., O'Nions, R.K., Óskarsson, N., and Oxburgh, E.R., 1983, Helium, oxygen, strontium and neodymium isotopic relationships in Icelandic volcanics: Earth and Planetary Science Letters, v. 66, p. 125–136, doi:10.1016/0012-821X(83)90131-0.

Constantin, M., Hékinian, R., Bideau, D., and Hébert, R., 1996, Construction of the oceanic lithosphere by magmatic intrusions: Petrological evidence from plutonic rocks formed along the fast-spreading East Pacific Rise: Geology, v. 24, p. 731–734, doi:10.1130/0091-7613(1996)024<0731:COTOLB>2.3.CO;2.

Cullen, A., Vicenzi, E.P., and McBirney, A.R., 1989, Plagioclase-ultraphyric basalts of the Galapagos archipelago: Journal of Volcanology and Geothermal Research, v. 37, p. 325–337, doi:10.1016/0377-0273(89)90087-5.

Dick, H.J.B. et al., 2002, Primary silicate mineral chemistry of a 1.5-km section of very slow spreading lower ocean crust: ODP Hole 735B, Southwest Indian Ridge: Proceedings of the Ocean Drilling Program, Scientific Results, v. 176, doi:10.2973/odp.proc.sr.176.001.2002.

Faak, K., and Gillis, K.M., 2016, Slow cooling of the lowermost oceanic crust at the fast-spreading East Pacific Rise: Geology, v. 44, p. G37353.1, doi:10.1130/G37353.1.

Gaetani, G.A., and Grove, T.L., 1998, The influence of water on melting of mantle peridotite: Contributions to Mineralogy and Petrology, v. 131, p. 323–346, doi:10.1007/s004100050396.

Gale, A., Langmuir, C.H., and Dalton, C.A., 2014, The Global Systematics of Ocean Ridge Basalts and their Origin: Journal of Petrology, v. 55, p. 1051–1082, doi:10.1093/petrology/egu017.

Ghiorso, M.S., and Sack, R.O., 1995, Chemical mass transfer in magmatic processes IV. A

revised and internally consistent thermodynamic model for the interpolation and extrapolation of liquid-solid equilibria in magmatic systems at elevated temperatures and pressures: Contributions to Mineralogy and Petrology, v. 119, p. 197–212, doi:10.1007/BF00307281.

Grove, T.L., Kinzler, R.J., and Bryan, W.B., 1992, Fractionation of Mid-Ocean Ridge Basalt (MORB), *in* Mantle Flow and Melt Generation at Mid-Ocean Ridges, Geophysical Monograph 71, Washington D.C., American Geophysical Union, p. 281–310.

Gurenko, A.A., and Chaussidon, M., 1995, Enriched and depleted primitive melts included in olivine from Icelandic tholeiites: Origin by continuous melting of a single mantle column: Geochimica et Cosmochimica Acta, v. 59, p. 2905–2917, doi:10.1016/0016-7037(95)00184-0.

Husen, A., Almeev, R.R., and Holtz, F., 2016, The Effect of H_2O and Pressure on Multiple Saturation and Liquid Lines of Descent in Basalt from the Shatsky Rise: Journal of Petrology, v. 57, p. 309–344, doi:10.1093/petrology/egw008.

Jarosewich, E., Gooley, R., and Husler, J., 1987, Chromium Augite - A New Microprobe Reference Sample: Geostandards and Geoanalytical Research, v. 11, p. 197–198, doi:10.1111/j.1751-908X.1987.tb00027.x.

Jarosewich, E., Nelen, J.A., and Norberg, J.A., 1980, Reference samples for electron microprobe analysis: Geostandards Newsletter, v. 4, p. 43–47.

Koga, K.T., Kelemen, P.B., and Shimizu, N., 2001, Petrogenesis of the crust-mantle transition zone and the origin of lower crustal wehrlite in the Oman ophiolite: Geochemistry, Geophysics, Geosystems, v. 2, doi:10.1029/2000GC000132.

Kohut, E.J., and Nielsen, R.L., 2003, Low-pressure phase equilibria of anhydrous anorthite-bearing mafic magmas: Geochemistry, Geophysics, Geosystems, v. 4, p. 1–27, doi:10.1029/2002GC000451.

Kress, V.C., and Carmichael, I.S.E., 1991, The compressibility of silicate liquids containing Fe_2O_3 and the effect of composition, temperature, oxygen fugacity and pressure on their redox states: Contributions to Mineralogy and Petrology, v. 108, p. 82–92, doi:10.1007/BF00307328.

Lange, A.E., Nielsen, R.L., Tepley, F.J., and Kent, A.J.R., 2013, The petrogenesis of plagioclase-phyric basalts at mid-ocean ridges: Geochemistry, Geophysics, Geosystems, v. 14, p. 3282–3296, doi:10.1002/ggge.20207.

Lissenberg, C.J., MacLeod, C.J., Howard, K.A., and Godard, M., 2013, Pervasive reactive melt migration through fast-spreading lower oceanic crust (Hess Deep, equatorial Pacific Ocean): Earth and Planetary Science Letters, v. 361, p. 436–447, doi:10.1016/j.epsl.2012.11.012.

Maclennan, J., 2008, Lead isotope variability in olivine-hosted melt inclusions from Iceland: Geochimica et Cosmochimica Acta, v. 72, p. 4159–4176, doi:10.1016/j.gca.2008.05.034.

Maclennan, J., McKenzie, D., Grönvold, K., Shimizu, N., Eiler, J.M., and Kitchen, N., 2003, Melt mixing and crystallization under Theistareykir, northeast Iceland: Geochemistry,

Geophysics, Geosystems, v. 4, p. 1–40, doi:10.1029/2003GC000558.

Namur, O., Charlier, B., Toplis, M.J., and Vander Auwera, J., 2012, Prediction of plagioclase-melt equilibria in anhydrous silicate melts at 1-atm: Contributions to Mineralogy and Petrology, v. 163, p. 133–150, doi:10.1007/s00410-011-0662-z.

Neave, D.A., Bali, E., Guðfinnsson, G.H., Halldórsson, S.A., Kahl, M., Schmidt, A.-S., and Holtz, F., 2019a, Clinopyroxene–liquid equilibria and geothermobarometry in natural and experimental tholeiites: the 2014–2015 Holuhraun eruption, Iceland: Journal of Petrology, v. 60, p. 1653–1680, doi:10.1093/petrology/egz042.

Neave, D.A., Maclennan, J., Hartley, M.E., Edmonds, M., and Thordarson, T., 2014, Crystal storage and transfer in basaltic systems: the Skuggafjöll eruption, Iceland: Journal of Petrology, v. 55, p. 2311–2346, doi:10.1093/petrology/egu058.

Neave, D.A., Namur, O., Shorttle, O., and Holtz, F., 2019b, Magmatic evolution biases basaltic records of mantle chemistry towards melts from recycled sources: Earth and Planetary Science Letters, v. 520, p. 199–211, doi:10.1016/j.epsl.2019.06.003.

Neave, D.A., Passmore, E., Maclennan, J., Fitton, J.G., and Thordarson, T., 2013, Crystal-melt relationships and the record of deep mixing and crystallization in the AD 1783 Laki eruption, Iceland: Journal of Petrology, v. 54, p. 1661–1690, doi:10.1093/petrology/egt027.

Neave, D.A., Shorttle, O., Oeser, M., Weyer, S., and Kobayashi, K., 2018, Mantle-derived trace element variability in olivines and their melt inclusions: Earth and Planetary Science Letters, v. 483, p. 90–104, doi:10.1016/j.epsl.2017.12.014.

Passmore, E., 2009, Feeding large eruptions: crystallisation, mixing and degassing in Icelandic magma chambers: University of Edinburgh, 379 p.

Peate, D.W., Baker, J.A., Jakobsson, S.P., Waight, T.E., Kent, A.J.R., Grassineau, N. V., and Skovgaard, A.C., 2009, Historic magmatism on the Reykjanes Peninsula, Iceland: A snap-shot of melt generation at a ridge segment: Contributions to Mineralogy and Petrology, v. 157, p. 359–382, doi:10.1007/s00410-008-0339-4.

Putirka, K.D., 2008, Thermometers and Barometers for Volcanic Systems: Reviews in Mineralogy and Geochemistry, v. 69, p. 61–120, doi:10.2138/rmg.2008.69.3.

R Development Core Team, 2016, R: A Language and Environment for Statistical Computing: R Foundation for Statistical Computing,.

Sanfilippo, A., Dick, H.J.B., Marschall, H.R., Lissenberg, C.J., and Urann, B., 2019, Emplacement and High-Temperature Evolution of Gabbros of the 16.5°N Oceanic Core Complexes (Mid-Atlantic Ridge): Insights Into the Compositional Variability of the Lower Oceanic Crust: Geochemistry, Geophysics, Geosystems, v. 20, p. 46–66, doi:10.1029/2018GC007512.

Schuessler, J.A., Botcharnikov, R.E., Behrens, H., Misiti, V., and Freda, C., 2008, Oxidation state of iron in hydrous phono-tephritic melts: American Mineralogist, v. 93, p. 1493–1504, doi:10.2138/am.2008.2795.

Shorttle, O., and Maclennan, J., 2011, Compositional trends of Icelandic basalts: Implications for short-length scale lithological heterogeneity in mantle plumes: Geochemistry, Geophysics,

Geosystems, v. 12, p. 1–32, doi:10.1029/2011GC003748.

Sisson, T.W., and Grove, T.L., 1993, Experimental investigations of the role of H_2O in calc-alkaline differentiation and subduction zone magmatism: Contributions to Mineralogy and Petrology, v. 113, p. 143–166, doi:10.1007/BF00283225.

Stock, M.J., Howard, K.A., Geist, D., Neave, D.A., Buisman, I., Maclennan, J., Gleeson, M.L.M., and Bernard, B., 2020, Cryptic evolved melts beneath monotonous basaltic shield volcanoes in the Galápagos Archipelago: Nature Communications, v. 11, p. 3767, doi:10.1038/s41467-020-17590-x.

Valer, M., Bachèlery, P., and Schiano, P., 2017, The Petrogenesis of Plagioclase-ultraphyric Basalts from La Réunion Island: Journal of Petrology, p. 1–24, doi:10.1093/petrology/egx030.

Voigt, M., Coogan, L.A., and von der Handt, A., 2017, Experimental investigation of the stability of clinopyroxene in mid-ocean ridge basalts: The role of Cr and Ca/Al: Lithos, v. 274–275, p. 240–253, doi:10.1016/j.lithos.2017.01.003.

Whitaker, M.L., Nekvasil, H., Lindsley, D.H., and Difrancesco, N.J., 2007, The role of pressure in producing compositional diversity in intraplate basaltic magmas: Journal of Petrology, v. 48, p. 365–393, doi:10.1093/petrology/egl063.

Whitaker, M.L., Nekvasil, H., Lindsley, D.H., and McCurry, M., 2008, Can crystallization of olivine tholeiite give rise to potassic rhyolites? - An experimental investigation: Bulletin of Volcanology, v. 70, p. 417–434, doi:10.1007/s00445-007-0146-1.

Yang, H.-J., Kinzler, R.J., and Grove, T.L., 1996, Experiments and models of anhydrous, basaltic olivine-plagioclase-augite saturated melts from 0.001 to 10 kbar: Contributions to Mineralogy and Petrology, v. 124, p. 1–18, doi:10.1007/s004100050169.